Optics Letters

Electrically pumped ultraviolet lasing in polygonal hollow microresonators: investigation on optical cavity effect

Zhifeng Shi,[1] Ying Li,[1] Yuantao Zhang,[2] Di Wu,[1] Tingting Xu,[1] Baolin Zhang,[2] Lei Liang,[3] Xinjian Li,[1,*] and Guotong Du[2]

[1]Department of Physics and Laboratory of Material Physics, Zhengzhou University, Daxue Road 75, Zhengzhou 450052, China
[2]State Key Laboratory on Integrated Optoelectronics, College of Electronic Science and Engineering, Jilin University, Qianjin Street 2699, Changchun 130012, China
[3]State Key Laboratory of Luminescence and Applications, Changchun Institute of Optics, Fine Mechanics and Physics, Chinese Academy of Sciences, Dongnanhu Road 3888, Changchun 130033, China
*Corresponding author: lixj@zzu.edu.cn

Received 3 October 2016; revised 10 October 2016; accepted 10 October 2016; posted 7 November 2016 (Doc. ID 277859); published 30 November 2016

Electrically driven ultraviolet lasing was realized in two-dimensional ZnO nanowall networks from Au/MgO/n-ZnO/n-GaN/In structure, and whispering gallery type resonant modes are responsible for the lasing action. We present a comparative study on lasing action based on nanowall networks with different micro-hole sizes. The representative diode (Device II) with a moderate micro-hole size exhibits an ultralow threshold current density of 1.01 A/cm^2, and the lasing action can be sustained at a temperature up to ~413 K, showing a good temperature tolerance. Moreover, the corresponding characteristic temperature for Device II was derived as ~91.4 K. It can be qualitatively anticipated that this work will provide instructive guidelines for fabrication and development of high-performance ultraviolet laser diodes by using two-dimensional ZnO nanowall networks as the lasing gain media. © 2016 Optical Society of America

OCIS codes: (160.4670) Optical materials; (140.3460) Lasers; (160.4236) Nanomaterials.

https://doi.org/10.1364/OL.41.005608

Recently, an urgent requirement of the ultraviolet (UV) semiconductor laser has motivated our intensive research in ZnO because of its wide bandgap and large exciton binding energy at room temperature (RT) [1,2]. However, the far-ranging application of ZnO-based UV laser diodes (UV-LDs) has been delayed by the difficulties in acquiring high-quality ZnO films and stable p-ZnO. Typically, the devices were mostly established based on n-ZnO-based heterojunction and metal/insulator/semiconductor (MIS) junction, in which ZnO nanostructures were employed as the gain media [3–5]. As a novel nanostructure, the research on two-dimensional (2D) ZnO nanowall networks (NNWs) is rare, especially on the UV-LDs. This is mainly due to a distinct microstructure of NNWs in which self-formed cavities developed from the adjacent nanowalls are formed. The microresonators can greatly enhance the optical gain and induce an amplified spontaneous emission [6]. Besides, the NNWs have a better chance to release heat because of their large surface-volume ratio. Thus, low-threshold lasing with a good temperature tolerance could be expected. In our previous work, electrically pumped UV lasing based on ZnO/MgO NNW structures has been demonstrated [7], but the effect of micro-hole size (different micro-hole sizes produce different microresonators) in ZnO NNWs on device performance (e.g., threshold current, characteristic temperature, and critical working temperature) has not been investigated further. In this study, ZnO NNWs with different micro-hole sizes were grown on n-GaN/c-Al_2O_3 substrates, and further MIS-type LDs were fabricated. We carefully checked the effect of micro-hole size on the lasing characteristics of UV-LDs. The experimental studies showed that the LD constructed with ZnO NNWs with a larger micro-hole size has a larger lasing threshold, a higher characteristic temperature, and a lower critical working temperature. The underlying reasons for the observed trends were discussed based on experimental results and theoretical analysis. It is believed that the obtained results will provide valuable information for the design of high-performance ZnO-based LDs.

In this work, a metal-organic chemical vapor deposition system was used for the growth of ZnO NNWs. Diethylzinc (DEZn) and oxygen gas (O_2) were used as the reactants. A two-step growth method was employed—a low-temperature nucleation layer with c-plane grains and subsequent high-temperature growth—to obtain ZnO NNWs. In this growth experiment, the O_2 was typically supplied with three flow rate points (8.0, 11.1, and 13.3 mmol/min) and the flow rate of DEZn (11.4 μmol/min) remained constant. Finally, three ZnO products with the thickness of ~2.0 μm were prepared;

the corresponding surface morphology is shown in Figs. 1(a)–1(c). By comparison, one can observe a controllable morphology evolution law. The average micro-hole size formed among the interconnected nanowalls significantly increases with the O_2 flow rate and reaches 0.8 μm at the O_2 flow ratio of 13.3 mmol/min. After the ZnO growth process, the Au/MgO/n-ZnO/n-GaN MIS structure was prepared by magnetron sputtering (MgO, ~40 nm) and thermal evaporation (Au, ~30 nm) methods. Three MIS-type diodes (denoted as Devices I, II, and III) were fabricated to check the effect of micro-hole size of NNWs on the device performance. The schematic diagram of the device structure is illustrated in Fig. 1(d), and the typical current-voltage (I–V) characteristics of constructed MIS-type diodes are shown in Fig. 1(e). Obvious nonlinear behaviors were observed from three diodes although the leak currents are relatively large [3,7]. Moreover, an additional observation is that the slope of the I–V curve at forward bias gradually decreased with the increase of micro-hole size in ZnO NNWs, indicating a difference in the series resistance of three diodes. The above phenomenon can be explained by the variation of distribution density of ZnO NNWs.

Electroluminescence (EL) of the three LDs was performed to demonstrate the lasing action. Herein, we take Device II as the research object considering that three diodes display UV lasing and they also share similar spectra features. As shown in Fig. 2, the EL spectra of Device II at different currents are plotted for comparison. At the low currents (5.4 and 7.0 mA), an emission at ~380 nm can be detected, corresponding to the near-band-edge emission of ZnO. As the current reaches 8.0 mA, some sharp peaks emerge superposing on the emission band. With a further increase of the current to 9.5 mA and above, these discrete peaks become sharper and more peaks show up. The appearance of such sharp peaks implies a lasing action, which is further evidenced by the simultaneous linewidth narrowing and superlinear increase of EL intensity at pumping density above the threshold as shown in the inset of Fig. 2. Fitting the light output versus current plot to the expected *S*-curve model gives a lasing threshold of 7.8 mA (1.01 A/cm^2).

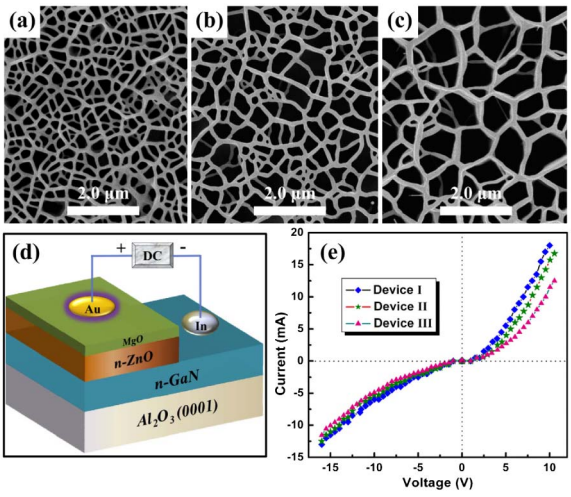

Fig. 1. (a)–(c) SEM images of ZnO NNWs with different micro-hole sizes. (d) Schematic diagram of the Au/MgO/n-ZnO NNWs/n-GaN/In structured diode. (e) I–V curves of the studied diodes.

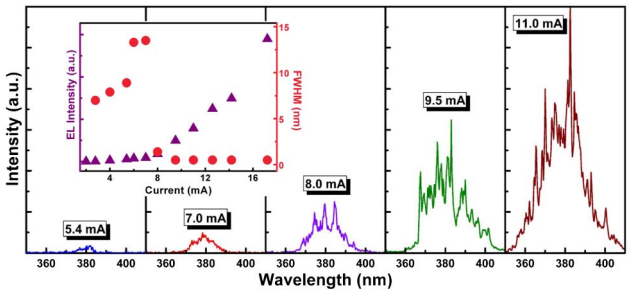

Fig. 2. EL spectra of Device II under different currents. The inset shows the EL intensity and FWHM of the lasing peaks versus driving currents.

Besides, near-field optical microscope images of Device II at above-threshold currents were recorded for a vivid presentation of the lasing nature (not shown here). Many bright spots randomly distribute across the entire contact area. Herein, we attributed the above-mentioned spots to the isolated resonators formed in the 2D ZnO NNWs. For such a morphology structure, the formation of optical microresonators is of great randomness due to the nonuniform distribution of micro-holes in shape and size, none of which is deliberately favored to obtain a sufficient optical gain among the first and which even enable lasing. Figure 3(a) depicts the schematic views of a closed-loop light oscillation (hexagon is an example) proceeding in the interconnected nanowalls. In order to characterize the cavity field distribution and photon localization in the microresonators, 2D finite-difference time-domain methods were carried out to calculate the electrical field distribution. The three insets in Fig. 3(a) show the simulated resonance patterns of proposed tetragon, pentagon, and hexagon microstructures. Distinct standing wave field distribution induced by the optical feedback at the air/ZnO interface can be formed, indicating the rationality of the proposed polygonal hollow microresonators in theory.

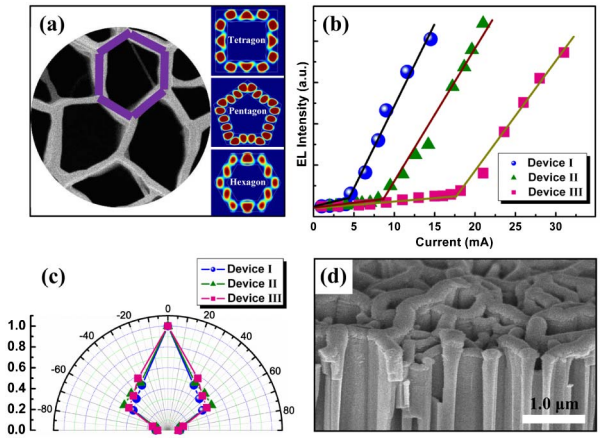

Fig. 3. (a) Schematic views of approximate hexagon structure defined by interconnected nanowalls. The right insets depict the numerically computed electric-field energy distribution in proposed microresonators. (b) Dependencies of EL intensity on the injection current for three LDs. (c) Angle-dependencies of the EL intensity for three LDs in the polar coordinate system. (d) Cross-sectional SEM image of ZnO NNWs (micro-hole size: ~0.8 μm) coated by MgO layer.

Additionally, the dependence of the EL intensity against current for Devices I and III was plotted in Fig. 3(b) and was put together with that of Device II to assess the effect of micro-hole size on the lasing threshold. An obvious trend can be observed: the diode constructed with NNWs with a larger micro-hole size has a larger lasing threshold. Such a trend is just the opposite of traditional whispering gallery mode (WGM) [8–10], in which the lasing threshold is inversely proportional to the cavity size. Understanding the underlying reasons seems challenging because the WGM is also responsible for the lasing observed in our case. Herein, the possible reasons were discussed, mainly considering two aspects. First, the nanowalls in Device I have a larger distribution density, so the injection current density should be smaller than that of Device III on the premise of a same Au electrode. However, considering the fact that the interconnected walls in a resonator do not share the same height and width, we have reason to believe that the uniformity of current injection for a microresonator is really not perfect, and especially the larger the size of the microresonator, the more significant the nonuniformity of current injection. In other words, only if the current is at a higher level for Device III is the optical gain obtained along the laser cavities sufficient to enable lasing. Second, the polygonal microresonators do not have a regular model; therefore, the light transmission/oscillation process would be accompanied by a high light loss. Such a phenomenon is more significant for the LDs with a larger micro-hole size, and a "softer" threshold [Fig. 3(b)] for Device III is the direct evidence because a "soft" threshold behavior in semiconductor lasers is presumably due to a large light loss and/or a relatively strong level of spontaneous emission [11,12]. Therefore, it is reasonable that an elevated pumping power is required to compensate for the optical loss to enable lasing for Device III.

In order to get more information on the lasing characteristics of the LDs, we performed the emission profiles of three LDs to investigate the effect of micro-hole size on the direction of laser output [Fig. 3(c)]. Note that the emission profiles were drawn based on the angular-dependent EL intensity. The angle θ was the detection angle between the devices' normal direction and the detector. Although the sharp peaks symbolized show lasing can still be detected in all six recording configurations, the emission intensity is dramatically decreased from 0° to 90° (−90°). Because the direction of laser output at 0° is not deliberately favored, the maximum emission intensity detected from the upper Au electrode seems very interesting. From the typical morphology characteristics of ZnO NNWs coated by an MgO layer [Fig. 3(d)], we recognize that the constructed MgO/ZnO bilayer structure is characterized by a nano-rough air/MgO interface, which can presumably modify the escape process of photons not only for an increased light extraction area but also for a light scattering effect at a rough air/MgO interface.

Moreover, temperature-dependent EL measurement was carried out to verify the sensitivity of the lasing to temperature. Over the course of measurement (using Device II as the research object), we adjusted the working temperature of Device II from RT to 413 K and the current was set to 21 mA. As shown in Fig. 4, a regular change can be found with increasing the working temperature. Owing to the heating-induced bandgap shrinkage, the overall lasing emission is slightly red shifted [13]. It should be pointed out that the coherent lasing can be sustained at 413 K, although the sharp

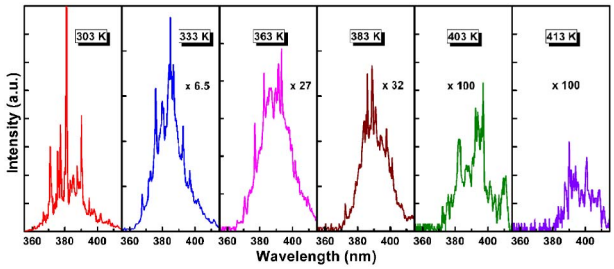

Fig. 4. Surface EL spectra of Device II at a fixed current of 21 mA measured at different working temperature.

peaks diminish and their intensities decrease. Above the critical temperature point, no lasing peaks can be observed, and meanwhile the emission intensity is dramatically decreased. Generally, the heating effect will inevitably give rise to a rapid proliferation of structural defects producing a large number of nonradiative recombination centers. Thus, the probability of nonradiative recombination is likely to increase in proportion to the temperature. The direct consequence is that the lasing ceases or no reliable light output can be observed normally.

As we stated above, at elevated temperatures the reduced carrier injection efficiency and radiative recombination probability will impede the UV lasing and, therefore, a higher pumping intensity is required to compensate for the heating-induced loss, thus allowing for optical gain and amplified spontaneous emission at high temperatures. As shown in Fig. 5(a), we plotted the light-current curves of Device II operating at three representative temperature points (303, 363, and 403 K), and the lasing threshold was well defined by the "kink" in the curves. One can see that the lasing threshold is 7.8 mA at RT, it increases to 12.8 mA at 363 K, and further increases to 19.6 mA at 403 K featuring a regular sensitivity to the temperature change.

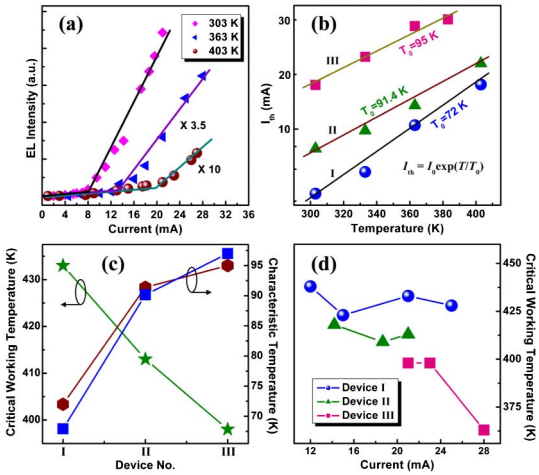

Fig. 5. (a) Dependence of the EL intensity for Device II on current at three different temperature points. (b) Variation of the lasing threshold against temperature on a semi-logarithmic scale for three diodes. (c) Variation of the critical working temperature and T_0 [theoretical estimation (wine-red hexagon) and experimental validation (blue square)] versus the device number. (d) Critical working temperatures of three LDs measured at different above-threshold currents.

One way to evaluate the operating stability of LDs is to calculate their characteristic temperature, which reflects the sensitivity of the lasing threshold to temperature [14]. As shown in Fig. 5(b), the variations of the lasing threshold for three LDs versus temperature were plotted, and a good fit for the experimental data was obtained by the formula $I_{th} = I_0 \exp(T/T_0)$ [15], where I_0 is the threshold at zero K and T_0 is the characteristic temperature. The best fittings yield T_0 values of ~72, 91.4, and 95 K for Devices I, II, and III. Note that the theoretical calculation of T_0 in our case was further experimentally validated. In the experimental validation for T_0, the LDs were mounted on a copper heat sink by using thermally conductive silicone as the adhesion layer. The copper heat sink was heated by a heating plate and the temperature can be adjusted from RT to 450 K. Owing to the high thermal conductivity of the copper heat sink and thermally conductive silicone, the surface temperature of the copper heat sink can be approximately regarded as the working temperature of the device. During the measurement, a series of light-output-power versus injection-current-density curves was obtained at different temperatures. By comparing the "kink" of the light-output-power versus injection-current-density curves, T_0 values of three diodes can be obtained. As shown in Fig. 5(c), the good agreement between the theoretical estimation (wine-red hexagon) and experimental validation (blue square) on T_0 confirmed our results although a ~3.5% deviation still exists. As for the deviation between the theoretical estimation and experimental validation values, two possible reasons are summarized and listed as follows: (1) the experimental validation on T_0 was carried out in air conditioning. In the testing process, an imperceptible change in the environment's temperature will lead to an undesired measuring error, which is nearly unavoidable, and (2) in our case, the LDs were fabricated based on 2D ZnO NNWs. Owing to the reason that the interconnected walls do not share the same height and width, the deposited MgO and Au layers will suffer from a nonuniform thickness, which is different from the traditional planar heterostructures. However, the theoretical estimation of T_0 was derived without completely considering the layer nonuniformity. In addition, the reproducibility of the experimental measured data (T_0) was also verified by randomly selecting six device units (take Device II as the research object, not shown here) for identical measurement, and the obtained data is irregularly distributed with an average T_0 of about 90.96 K. Considering the different morphology of ZnO NNWs in three LDs, we therefore attribute the higher T_0 in Device III to the larger micro-hole size of NNWs. A larger micro-hole size implies an increased surface-volume ratio, thus heat from a device could be rapidly released and an improved stability can be expected. While the critical working temperature for the three LDs shows an opposite trend [Fig. 5(c)], such a variation trend is well consistent with the change of lasing threshold of the three LDs. It is reasonable that a high threshold limited for continuous-wave lasing should be determined by an increased heating effect, and a low critical working temperature is therefore required to weaken the heating-induced loss.

The above discussion leads to an interesting question: Can the critical working temperature be availably elevated by increasing the pumping power? Theoretically, a high optical gain could be guaranteed if the LD is driven at a high input power. However, this is a double-edged sword because device operation at a high pumping power is bound to induce an additional heating effect, and heating-induced loss will impede the UV lasing because the required pumping energy for stimulated emission could be consumed with the undesired nonradiative recombination. Therefore, in a sense, the pumping power applied in the LD does not necessarily relate to its critical working temperature. We performed three groups of experiments to investigate the relation of critical working temperature with pumping power. As shown in Fig. 5(d), the calculated values of T_0 are distributed irregularly and show their independence from the driving current.

In summary, MIS-type LDs based on 2D ZnO NNWs were demonstrated, and we performed a comparative investigation to check the effect of micro-hole size in ZnO NNWs on the lasing characteristics of the UV-LDs. The experimental studies showed that the LD constructed with ZnO NNWs with a larger micro-hole size has a larger lasing threshold, a higher T_0, and a lower critical working temperature. The underlying reasons for the observed trends were discussed. It can be qualitatively anticipated that this work will provide instructive guidelines for fabrication of high-performance UV-LDs based on ZnO NNWs and provide additional understanding on the lasing characteristics of such diodes.

Funding. National Natural Science Foundation of China (NSFC) (11604302, 61605174, 61176044, 11504331); China Postdoctoral Science Foundation (2015M582193); Science and Technology Research Project of Henan Province (162300410229); Postdoctoral Research Sponsorship in Henan Province (2015008); Zhengzhou University (1521317001, 1512317003).

REFERENCES

1. M. H. Huang, S. Mao, H. Feick, H. Yan, Y. Wu, H. Kind, E. Weber, R. Russo, and P. Yang, Science **292**, 1897 (2001).
2. H. B. Zeng, G. T. Duan, Y. Li, S. Yang, X. X. Xu, and W. P. Cai, Adv. Funct. Mater. **20**, 561 (2010).
3. H. Zhu, C. X. Shan, B. Yao, B. H. Li, J. Y. Zhang, Z. Z. Zhang, D. X. Zhao, D. Z. Shen, X. W. Fan, Y. M. Lu, and Z. K. Tang, Adv. Mater. **21**, 1613 (2009).
4. S. Chu, M. Olmedo, Z. Yang, J. Y. Kong, and J. L. Liu, Appl. Phys. Lett. **93**, 181106 (2008).
5. X. Y. Ma, P. L. Chen, D. S. Li, Y. Y. Zhang, and D. R. Yang, Appl. Phys. Lett. **91**, 251109 (2007).
6. E. S. Jang, X. Y. Chen, J. H. Won, J. H. Chung, D. J. Jang, Y. W. Kim, and J. H. Choy, Appl. Phys. Lett. **97**, 043109 (2010).
7. Z. F. Shi, Y. T. Zhang, X. Cui, S. Zhuang, B. Wu, X. Dong, B. Zhang, and G. T. Du, Sci. Rep. **4**, 7180 (2014).
8. J. Dai, C. X. Xu, and X. W. Sun, Adv. Mater. **23**, 4115 (2011).
9. R. Chen, B. Ling, X. W. Sun, and H. D. Sun, Adv. Mater. **23**, 2199 (2011).
10. M. A. Zimmler, J. Bao, F. Capasso, S. Müller, and C. Ronning, Appl. Phys. Lett. **93**, 051101 (2008).
11. T. Nobis, E. M. Kaidashev, A. Rahm, M. Lorenz, and M. Grundmann, Phys. Rev. Lett. **93**, 103903 (2004).
12. C. Yuen, S. F. Yu, E. S. P. Leong, H. Y. Yang, S. P. Lau, and N. S. Chen, Appl. Phys. Lett. **86**, 031112 (2005).
13. H. Y. Yang, S. P. Lau, S. F. Yu, A. P. Abiyasa, M. Tanemura, T. Okita, and H. Hatano, Appl. Phys. Lett. **89**, 011103 (2006).
14. S. Bidnyk, T. J. Schmidt, Y. H. Cho, G. H. Gainer, and J. J. Song, Appl. Phys. Lett. **72**, 1623 (1998).
15. X. H. Yang, T. J. Schmidt, W. Shan, and J. J. Song, Appl. Phys. Lett. **66**, 1 (1995).

159.226.165.13 {ts '2017-06-22 23:44:32'}